Chemical Engineering Journal 433 (2022) 133194

Contents lists available at ScienceDirect

Chemical Engineering Journal

journal homepage: www.elsevier.com/locate/cej

CFD simulation and experimental comparison of bubble-induced convection during electrochemical water splitting

Gabriel Wosiak, Jeyse da Silva, Sthefany S. Sena, Renato N. de Andrade, Ernesto Pereira *

Chemistry Department, Federal University of São Carlos, 13565-905, São Carlos, SP, Brazil

ARTICLE INFO

Keywords:
Hydrogen
Electrolysis
Finite element simulation
Water splitting

ABSTRACT

The behavior of gas bubbles produced during electrochemical processes is of large interest because of the increase in cell overpotential induced by their production, the electrode surface covering by them and, finally, the detachment of these bubbles and their direct impact on the energy consumption during the reaction. In this work, we used coupled experimental and computational approaches to investigate bubble formation under those conditions where there are important convective effects. We have measured both normal and parallel velocity of the solution and built up a computational fluid dynamics (CFD) model. The results were compared to experimental data. Then, having the computational model validated by experimental data, we have simulated different conditions following bubble displacement. An important change of the surface covering is observed during the electrochemical reaction. Considering just the covering change, for example, there is up to 23 % increase comparing to the electrode edge and center.

1. Introduction

Both hydrogen-based energy storage systems and fuel cell-based mobility systems are interested in cost-effective large-scale hydrogen generation [1–3]. Water electrolysis is an important piece of technology for manufacturing the requisite of high purity hydrogen since, in addition to being a waste-free process, it can also be paired with renewable energy sources. Thus, making it the most sustainable way of manufacturing high purity hydrogen [4,5], also known as green hydrogen.

One of the key challenges in making water electrolysis economically viable is to increase process efficiency by lowering cell voltage, enhancing solution flow conditions, pressure, temperature, and developing new materials to reduce the activation by catalytic effects [6,7,7–10]. Most electrochemical processes, especially those involving water as part of the electrolyte, result in the formation of bubbles on the electrode surface [11–14], making it a topic of great interest due to many effects on the reaction efficiency. In some cases, the bubbles can cover a large portion of the electrode surface, reducing the number of active sites [15–17]. The buoyant force of the electrolyte's bubbles can increase the fluid flow of the electrolyte in most of these situations, improving convective mass transport and homogenizing the temperature field in the electrolyte [6,18]. For example, combining gas bubble movement with ultrasound perturbation can clean the solid–liquid interface [19–23].

During the formation and growth of bubbles, three overpotential components decrease the process efficiency: activation overpotential, ohmic overpotential, and concentration overpotential [24–27]. The existence of adherent bubbles lower the contact between electrode and electrolyte, affecting the activation overpotential. The ohmic overpotential is increased due to the obstruction of the electronic and/or ionic currents produced by both trapped and free bubbles [28,29]. The effect of convection in the efficiency of electrochemical process has been described by enhancing the species mixing [30,31], then reducing the concentration overpotential.

The modeling of multiphase flow by Finite Element Method (FEM) is well-established for applications in studies of heated surfaces and single or multi-channel gas-evolving electrochemical systems [32–41]. In general, the models are divided into simulations where the bubble size is negligible compared to the domain size, then the bubbles are treated as a dispersed phase. Besides, there are works that consider each bubble of the two or more non-miscible phases, which, in general, has a high computational cost to be performed. In the present work, we have used the first approach considering the decrease in the CFD model building and in the computational cost. Then, we validated the model with experimental results. [42–44].

Although the forming of bubbles in electrochemical processes has been described in several publications [45,46], their behavior has not been completely investigated to identify their direct impacts on the

* Corresponding author.
E-mail address: ernesto@ufscar.br (E. Pereira).

https://doi.org/10.1016/j.cej.2021.133194
Received 8 September 2021; Received in revised form 20 October 2021; Accepted 22 October 2021
Available online 7 November 2021

Nomenclature

Abbreviations

ASC	Average surface covering
CFD	Computational Fluid Dynamics
CSC	Center surface covering
FEM	Finite Element Method
HER	Hydrogen Evolution Reaction
OER	Oxygen Evolution Reaction
SAV	Surface Average Velocity

Symbols

$\mathbf{I}$	Identity matrix
$\mathbf{u}_g$	Gas velocity ($m\,s^{-1}$)
$\mathbf{u}_l$	Liquid velocity ($m\,s^{-1}$)
$\mathbf{u}_{drift}$	Drift velocity ($m\,s^{-1}$)
$\mathbf{u}_{slip}$	Slip velocity ($m\,s^{-1}$)
μ_l	Dynamic viscosity of the liquid (Pa s)
μ_T	Turbulent viscosity (Pa s)
Φ_g	Gas mass flux ($kg\,cm^{-2}\,s^{-1}$)
ϕ_g	Gas phase volume fraction (%)
ϕ_l	Liquid phase volume fraction (%)
ρ_l	Liquid density ($kg\,m^{-3}$)
d_b	Bubble diameter (m)
E^0	Standard potential (V)
j	Applied current density ($mA\,cm^{-2}$)
M_g	Molecular weight of gas ($kg\,mol^{-1}$)
n_e	Number of electrons
t	Time (s)
Vx	x component of velocity vector ($cm\,s^{-1}$)
Vy	y component of velocity vector ($cm\,s^{-1}$)

Physical constants

$\mathbf{g}$	Gravitational constant ($9.806\,65\,m\,s^{-2}$)
F	Faraday constant ($96\,485.3329\,C\,mol^{-1}$)

efficiency of water electrolysis. In this way, in this work we coupled both experimental and computational techniques in a unique form to model the bubble detachment, and its effect on the solution flow. Then, we measured the impact on the surface covering during water splitting, as well as their influence on convection and changes in the electrolyte concentration, an approach that is supported by the experimental data.

2. Experimental setup

The observation of the bubble formation was performed through a temporal series of images, i.e., making a movie of the experiments. The electrochemical flat window cell consists of three Pt electrodes, on the Working Electrode (WE) there was a 3 mm diameter Pt disk, positioned with the surface up to the solution to allow the bubbles to come off perpendicularly with no other effect but the external atmospheric pressure. We used two Pt grids as auxiliary electrodes positioned symmetrically to the working electrode, to keep the electric field as uniform as possible. The full experimental setup is presented in Fig. 2. $0.1\,mol\,L^{-1}$ H_2SO_4 was used as supporting electrolyte for the acid medium and $0.1\,mol\,L^{-1}$ KOH for the alkaline one. The recording setup was a Motorola One Vision smartphone (1920 × 1080, with frame rate of $60\,s^{-1}$) positioned in front the cell. A special care was taken to have constant illumination of the setup using two LED floodlights (30 W) to make an easy image data quantification. The experiments were

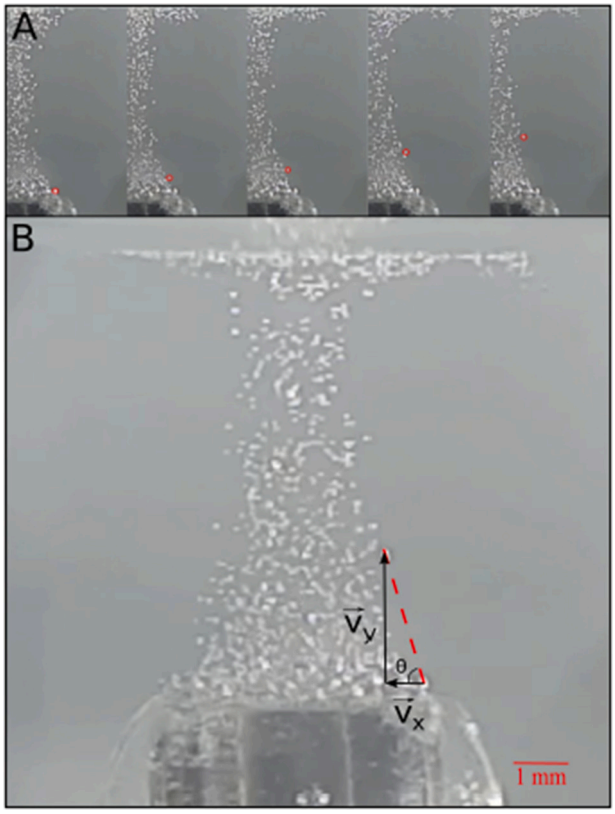

Fig. 1. Bubble flow pattern during water electrolysis at $100\,mA\,cm^{-2}$ with the (A) velocity vector components scheme and (B) single red-circled bubble during sequential frames.

performed under galvanostatic mode, changing the current density, $50\,mA\,cm^{-2}$ and $100\,mA\,cm^{-2}$. To study both H_2 and O_2 gases, we applied cathodic and anodic signals respectively to the WE.

For bubble velocity measurements, five random bubbles formed at the electrode edge were chosen and had their trajectories accompanied frame-by-frame (time) for each experiment, as shown in Fig. 1A as a single red-circled bubble along with the frames. To analyze the data, we measured the relative position of these bubbles until their lateral displacement vanishes, and then the velocity vector was decomposed into vertical (v_x) and horizontal (v_y) components, as shown in Fig. 1B. The whole data and procedure can be found at the Supporting Material including statistical parameters.

3. Simulations

3.1. Model

There are two main approaches to model two-phase flow: (i) separated multiphase flow models, that are used when the size of the bubbles is of the order of magnitude of the model domain; and (ii) a simpler approach: a dispersed flow, for bubbly flows with small bubbles. In this work, we used the last one which, as described above, has been validated by experimental data. For the calculation of transport of bubbles in the solution, this interface takes the average concentration of bubbles instead of looking each bubble in detail. This considerably reduces the computational cost for the calculation. In practice, it is a simplification of modeling in multiphase systems. The calculation time is about 20 min for each case in a computer operating with Ubuntu 20.04 LTS, and 128 GB of RAM and an Intel-Core i7-7800X as CPU.

The slip model is a pressure-drag balance considering small spherical bubbles by Hadamard–Rybczynski model [47,48], which considers the bubble diameter.

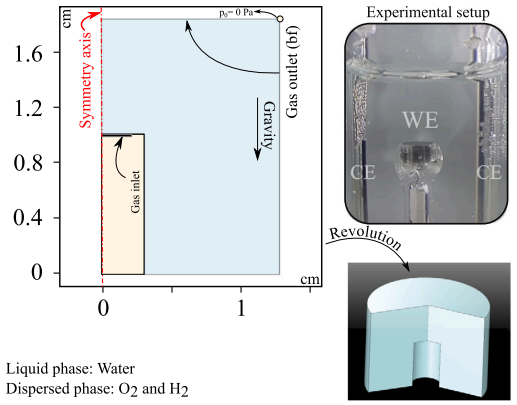

Fig. 2. Model description showing the simulated geometry based in experimental setup and the 3D revolution view.

In the bubbly flow interface, the momentum equation is

$$\phi_l \rho_l \frac{\partial \mathbf{u}_l}{\partial t} + \phi_l \rho_l \mathbf{u}_l \cdot \nabla \mathbf{u}_l = -\nabla p + \nabla \cdot \left[\phi_l(\mu_l + \mu_T)\left(\nabla \mathbf{u}_l + \nabla \mathbf{u}_l^T - \frac{2}{3}(\nabla \cdot \mathbf{u}_l)\mathbf{I}\right)\right] + \phi_l \rho_l \mathbf{g} + \mathbf{F}\,, \quad (1)$$

where ϕ is the phase volume fraction (%), which provides the electrode covering, ρ is the liquid phase density ($kg^3\,m^{-1}$), $\mathbf{u}_l$ is the velocity vector for the liquid phase ($cm\,s^{-1}$), μ_l and μ_T are the liquid dynamic viscosity (Pa s) and the turbulent viscosity (Pa s), $\mathbf{I}$ is an identity matrix, $\mathbf{g}$ is the gravity vector ($m\,s^{-2}$) and $\mathbf{F}$ is any additional volume force in $N\,m^{-3}$.

We define liquid water as the continuous phase, taking account their density and dynamic viscosity, and for the dispersed phase, we used O_2 and H_2 gas density from COMSOL® Material Library. Two levels of bubble diameter was included in the design of experiments.

For a deeper interpretation of the experimental results, we created a finite element based model using the CFD module from COMSOL® Multiphysics 5.6 software and the geometry was based on the experimental setup using the bubbly flow (bf) with a $k-\epsilon$ turbulence model RANS type. This interface solves the model for $\mathbf{u}_l$ and p, and the effective gas density is given by multiplying the calculated gas density from the ideal gas law by the gas fraction (ϕ_g). The gas velocity is the sum of the components

$$\mathbf{u}_g = \mathbf{u}_l + \mathbf{u}_{\text{slip}} + \mathbf{u}_{\text{drift}} \quad (2)$$

$\mathbf{u}_{\text{slip}}$ is the relative velocity vector between the phases and $\mathbf{u}_{\text{drift}}$ is the drift velocity from the turbulence model, which includes a diffusive term in gas transport.

Fig. 2 shows the model used to simulate the experiment using the disk electrode as WE. The gas flux in the electrode boundary, $\boldsymbol{\Phi}_g$ ($kg\,cm^{-2}\,s^{-1}$), is defined as

$$\boldsymbol{\Phi}_g = \frac{jM_g}{Fn_e}\,, \quad (3)$$

where j is the applied current density ($mA\,cm^{-2}$) in the experimental electrolysis, M_g is the gas molecular weight, F is the Faraday constant and n_e is the number of electrons. It is important to note that the molar gas flux ($mol\,cm^{-2}\,s^{-1}$) for H_2 is two times larger than that of O_2 for the same current density.

4. Results and discussion

4.1. Experimental results

Fig. 1 describes the solution flow affected by the bubble detachment and movement into the solution. It is important to stress out that these bubbles do not move perpendicularly toward the solution surface but do it in a diagonal pathway which is indicated in the Figure. Such kind of displacement is related to the effect of bubbles in the solution movement. In the present case, although, under some experimental conditions, the observation of all bubbles in the surface is not easy. However, it is useful to measure the solution movement associated with bubble displacement in the solution. It is also important to note that the bubbles move towards the center, and not the opposite, forming a pattern similar to a "wedding dress". The visible bubbles allow good visualization of the electrolyte movement.

Table 1
x and y velocity components for experimental bubble flow. Units: j in $mA\,cm^{-2}$, V_x and V_y in $cm\,s^{-1}$.

Exp	Medium	Gas	j	V_x	V_y
1	Acid	H_2	100	0.42 ± 0.04	0.94 ± 0.12
2	Alkaline	H_2	50	0.26 ± 0.03	0.74 ± 0.04
3	Alkaline	O_2	50	0.12 ± 0.01	0.47 ± 0.08
4	Acid	H_2	50	0.24 ± 0.05	0.74 ± 0.13

The velocity of individual bubbles have been determined by decomposing the x and y velocity vector components, as shown in Fig. 1B. From the velocity calculations of single bubbles, it was possible to obtain the average x and y components of the velocity vector, as described in Table 1. More detailed data can be found on Supporting Material.

The largest x-direction velocity (V_x) is observed in acid media for H_2 gas and $100\,mA\,cm^{-2}$. This is an expected result because this condition has a greater amount of gas formed per unit time, which, as a consequence, enhances the fluid flow more strongly. Comparing experiments 1 and 4, with same pH conditions and gas type, V_x is doubled by doubling the flow. Besides, the angle formed decreases from an average value of 71.78 ± 2.68 to 64.94 ± 3.78, indicating that the slope in the formation of the narrowing of the bubble profile in experiment 1 is more accentuated. This behavior could be related to the increase in the flux of bubbles, as mentioned before, which makes those bubbles formed on the edge suffer a strong influence from the vortex pressure. Consequently, at small current, the observed slope has a larger angle.

Analyzing experiments 2 and 3, the effect of gas identity in the same solution and current can be evaluated. As expected, V_x is twice the value, considering the experimental error, for hydrogen, which could be associated with the reaction stoichiometry. However, this change is different for V_y. Although a precise reason cannot be extracted from the present data, we propose that the difference in gas densities, O_2 and H_2, which have consequence is the buoyancy force, is the main responsible for the observed result. It is important to note that the buoyancy force also depends on the height of water column above the bubble, that changes as the bubble rises. Due to its smaller density, hydrogen has a higher V_y value, which implies in a stronger fluid convective movement, enhancing the vortex pressure on the lateral displacement of the bubbling flow. For that reason, the smaller V_y for O_2 also results in its smaller lateral displacement, which is 26.9% lower than the hydrogen's one. This implies the largest angle observed from this lateral displacement of the O_2 bubbles, $75.18 \pm 1.85°$.

Although the medium, acid or alkaline, influences the water-splitting reaction, no significant differences were observed regarding the angle formed or the lateral displacement of bubbles resulting from the vortex formed in the solution. As can be seen comparing experiments 2 and 4, both conditions give an equivalent result for the velocity vector components. This experimental evidence helps us to built a simple physical model, once it is not necessary to describe the specific properties of the solution in the present work.

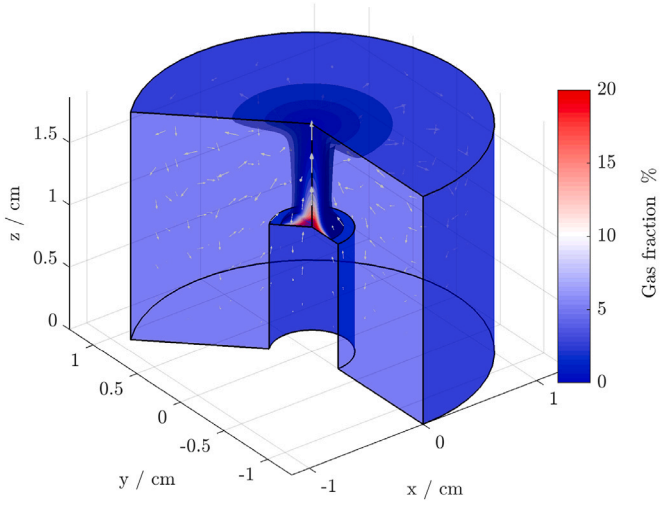

Fig. 3. Three-dimensional isosurface plot of gas fraction on the domain. White arrows represents the velocity vector direction. d_b=60 µm, j=75 mA cm^{-2} and t=2 s.

4.2. Bubble behavior and experimental validation

Fig. 3 shows an interactive (see online version) three-dimensional view of the steady-state bubble behavior. As soon as the bubbles rise they generate a convective flow that sweeps bubbles near electrode towards the center and results in a vertical velocity from the center of the electrode to the surface of the solution.

Fig. 4 shows that at the beginning of electrolysis, the formation of gas affects directly the velocity field over the electrode surface, where the heterogeneous processes occur, promoting forced convection in the solution. There are horizontal flux lines near the electrode surface that sweep the formed bubbles to the electrode center. As a consequence, the number of exposed active sites to the solution phase at the center is decreased compared to edge. This means that the covering and the concentration of gas bubbles is non-homogeneous over the surface. These experimental facts were used in our physical model. In the model, also presented in Fig. 4, the effect is observed due to the large number of the bubbles as well their displacement in the solution. The electrode body modifies the solution flow, giving it a V_x component which strong affects the bubbles displacement in the same solution, which characterizes a self-feed effect. When the bubbles reach the center, they flow to the top of the solution, causing turbulent movement in the whole fluid. A video is provided as a supplementary information section in order to understand Fig. 4 with more details.

Once the physical model was validated by the experimental data, we investigated different boundary conditions using simulation to evaluate the effect of asymmetrical flow solution on them. We investigated the following: current density, bubble size, and gas type.

As can be seen in Fig. 5(a), the fraction of gas covering the electrode surface tends to increase with decreasing bubble diameter. The same amount of gas can produce few big or many small bubbles. In the first case there is less contact between the electrode and the electrolyte. In cases where d_b is greater, the detachment of the bubbles occurs faster. On the other hand, with smaller d_b, there is time for the vortex to drag the bubbles towards the center where they coalesce, remaining longer near the surface.

The effect of current density is directly related to the produced gas amount. According to Faraday's laws of electrolysis, this amount depends on the reaction stoichiometry and the applied current density. In high amounts of formed gas, the bubbles end up staying longer on the electrode surface.

Fig. 5(b) shows the x component of the velocity vector for various conditions related to the electrode surface, which is related to the non-homogeneity of the bubble covering at the electrode surface.

Table 2
Line average gas fraction in different temperature and current density condition (SAV-Surface Average Velocity, CSC-Center Surface Covering, ASC-Average Surface Covering).

Exp	d_b	j (mA cm^{-2})	Gas	SAV (cm s^{-1})	CSC (%)	ASC (%)	CSC-ASC (%)
1	20	50	H2	1.06	16.3	9.36	6.89
2	100	50	H2	0.612	2.52	2.09	0.424
3	20	100	H2	1.38	29.2	16.9	12.3
4	100	100	H2	0.921	5.15	4.13	1.02
5	20	50	O2	1.39	29.5	17.0	12.5
6	100	50	O2	0.926	5.19	4.15	1.04
7	20	100	O2	1.84	53.8	30.7	23.2
8	100	100	O2	1.35	10.9	8.22	2.64
9	60	75	H2	1.08	9.72	6.34	3.38
10	60	75	O2	1.47	19.16	12.23	6.93

We can see that small bubbles can improve the electrolyte convection, and the current density also has a strong effect due to the amount of formed gas, i.e., the bubble-induced convection is higher at high currents. The nearer to the symmetry axis, the lower the x component should be, reaching zero at the symmetry axis, since its velocity at this point is given by the y component only. As the bubble is formed farther from the center of the electrode, the y component gains more importance, since there is a lateral displacement of it due to the vortex in the liquid phase.

For understanding the influence of the parameters on the bubble displacement and gas surface covering, Fig. 6 shows a DoE approach for analyzing the simulation results on different conditions, which is a reasonable approach considering the correspondence between experimental results and simulation model. The simulated results allow us to access the average velocity over the electrode surface (SAV) as well as the difference between the covering at the center and the average along the whole electrode (SAV-ASC).

The values presented in Table 2, i.e., the average value of the variables liquid velocity ($\mathbf{u}_l$), were used as starting values in the simulation to calculate Surface Average Velocity (SAV) and the gas phase volume fraction (ϕ_g), aiming to determine the Average Surface Covering (ASC) on the electrode surface boundary. The maximum (ϕ_g) value for all the simulated cases is at the electrode center, so we defined this value as Center Surface Covering (CSC), and took the difference between the CSC and ASC as the DoE response, in order to study how the solution convection influences the non-uniformity of the bubble concentration over the electrode.

For a multivariate view, Fig. 6(a) shows the relative contribution of the input parameters on the selected responses. The bubble diameter has the major negative contribution for both cases, that is, the larger the bubble, the slower is the convection, and, as a consequence, the difference between the covering at the center and the average is larger. The current density (B) is relatively more significant for the SAV. This effect is positive, that is, the larger the current density, the larger the surface liquid velocity. The greater the current, the less homogeneous is the gas distribution over the electrode. The formed gas also has a positive influence in both responses. We used H_2 as a lower level, and even the gas quantity is twice for this condition. The lower density of O_2 gas causes a higher displacement on the electrode surface. In Fig. 6(a), the histogram for the effects and the Pareto plots for both results investigated are presented. It is clear from the results that all the main effects of the variables current density, bubble size and gas kind are significant. In a different form, the cross effect of two and three variables are not significant. The bubble diameter decreases the average $V_{x(calc)}$ value, in other words, it decreases the vortex effect of the solution flow. As a consequence, the bubble covering also decreases, meaning that the asymmetry of surface covering also decreases. Current densities have an opposite effect, i.e., as the current is increased the asymmetric in both, $V_{x(calc)}$ and surface covering asymmetry increases. As the current density is increased the total number of bubbles is also

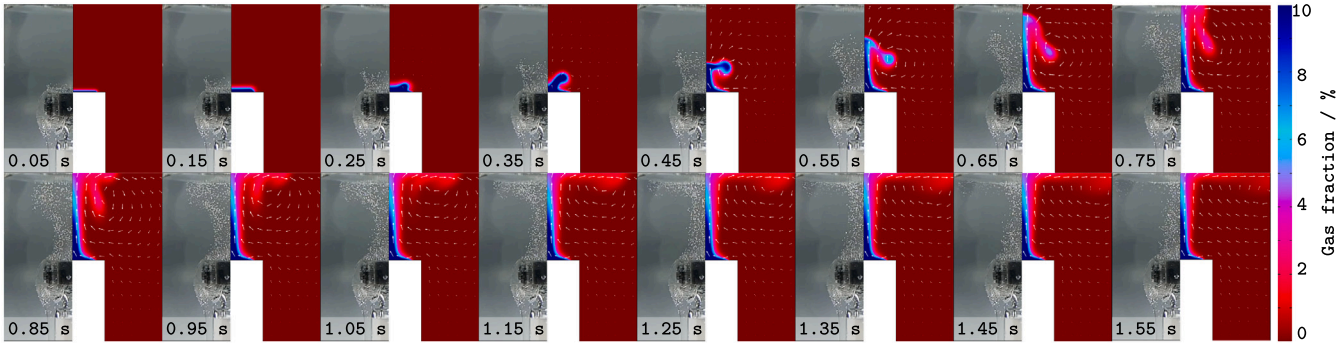

Fig. 4. Time-dependent simulation and experimental comparison of H_2 evolution showing the fluid velocity (white arrow) and the gas fraction in the domain. j=100 mA cm^{-2}, d_b=20 µm.

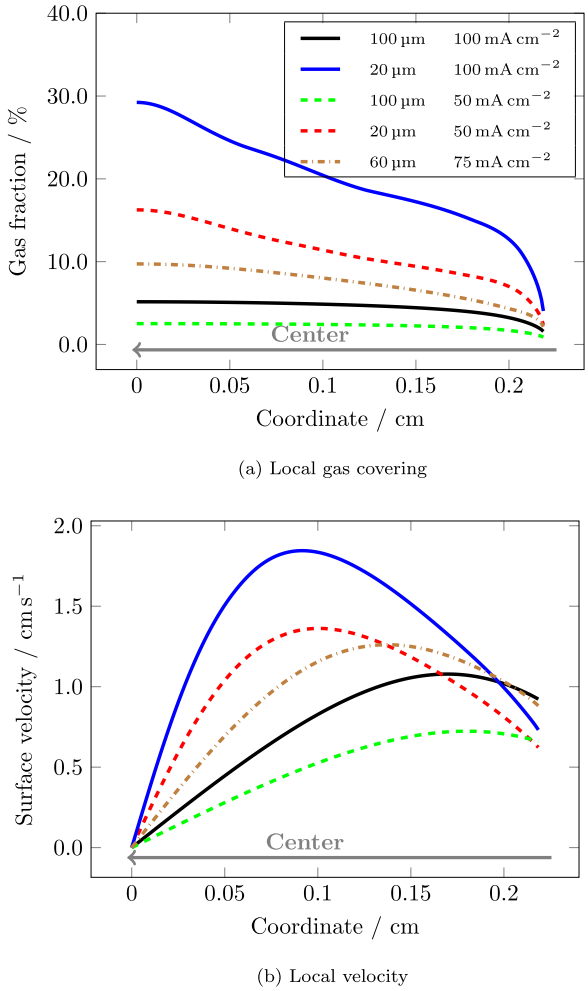

(a) Local gas covering

(b) Local velocity

Fig. 5. Simulated results for local variables obtained by taking the values in the electrode boundary for H_2 gas.

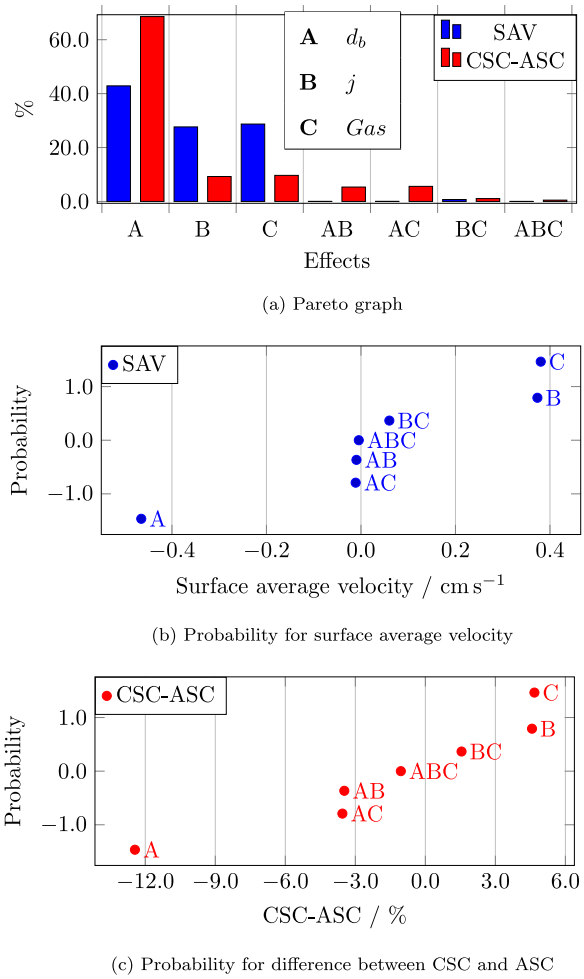

(a) Pareto graph

(b) Probability for surface average velocity

(c) Probability for difference between CSC and ASC

Fig. 6. DoE graphs for the average surface covering (ASC) and center surface covering (CSC) showing the relative contribution of the effects (d_b, j and *Gastype*).

expected to increase, and then, the effect on the solution flow narrowing is also increased as expected. Finally, the gas kind has a significant effect on the results presented in Fig. 6. Two important gas properties changes in these case: gas density and gas amount. Even though the model describes these properties explicitly, they are considered in the model whenever we use COMSOL's® Materials database. Although considering steady state conditions under atmospheric pressure could made suppose that these two gas behaves as ideal gas, this is not the case in the moment the are generated under electrochemical very strong electric field.

The similarity of Figs. 6(b) and 6(c) shows that the non-homogeneity of the surface covering is directly related to the horizontal velocity vectors near the electrode.

Finally, we have used both experimental and simulated results to investigate a large number of conditions in which the bubbles displacement in the solution leads to a non symmetric solution flow. The importance of the results is that it modifies in an important form

the bubble surface covering which certainly affects the water splitting reaction efficiency.

5. Conclusions

The transport of bubbles in the solution was simulated, corroborating experimental data. This simulation also allowed the observation of the electrode coating due to the bubbles in different boundary conditions, which has direct consequences on the efficiency of many electrochemical processes.

In light of the growing need to improve the hydrogen production process, this work proves to be useful for a deeper understanding of this component of the process (bubble formation) that received little attention in the past, but which, as our research shows, has a direct impact on the efficiency of hydrogen gas production.

Declaration of competing interest

The authors declare that they have no known competing financial interests or personal relationships that could have appeared to influence the work reported in this paper.

Acknowledgments

The support of this research by FAPESP, Brazil grants 2013/07296-2, 2014/50249-8, 2017/11986-5, 2018/24383-0, and 2019/27029-5), Shell, Brazil, CNPq, Brazil, and CAPES, Brazil (Code 001).

Appendix A. Supplementary data

Supplementary material related to this article can be found online at https://doi.org/10.1016/j.cej.2021.133194.

References

[1] C. Brussieux, P. Viers, H. Roustan, M. Rakib, Controlled electrochemical gas bubble release from electrodes entirely and partially covered with hydrophobic materials, Electrochim. Acta 56 (20) (2011) 7194–7201, http://dx.doi.org/10.1016/j.electacta.2011.04.104.

[2] I. Dincer, C. Acar, Review and evaluation of hydrogen production methods for better sustainability, Int. J. Hydrogen Energy 40 (34) (2014) 11094–11111, http://dx.doi.org/10.1016/j.ijhydene.2014.12.035.

[3] Y. Wang, S. Zhang, Economic assessment of selected hydrogen production methods: A review, Energy Sour. B 12 (11) (2017) 1022–1029, http://dx.doi.org/10.1080/15567249.2017.1350770.

[4] P.S. Epstein, M.S. Plesset, On the stability of gas bubbles in liquid-gas solutions, J. Chem. Phys. 18 (11) (1950) 1505–1509, http://dx.doi.org/10.1063/1.1747520.

[5] A. Moreno Soto, A. Prosperetti, D. Lohse, D. Van Der Meer, Gas depletion through single gas bubble diffusive growth and its effect on subsequent bubbles, J. Fluid Mech. 831 (2017) 474–490, http://dx.doi.org/10.1017/jfm.2017.623.

[6] X. Yang, F. Karnbach, M. Uhlemann, S. Odenbach, K. Eckert, Dynamics of single hydrogen bubbles at a platinum microelectrode, Langmuir 31 (29) (2015) 8184–8193, http://dx.doi.org/10.1021/acs.langmuir.5b01825.

[7] D. Deng, K.S. Novoselov, Q. Fu, N. Zheng, Z. Tian, X. Bao, Catalysis with two-dimensional materials and their heterostructures, Nature Nanotechnol. 11 (3) (2016) 218–230, http://dx.doi.org/10.1038/NNANO.2015.340.

[8] A. Angulo, P. van der Linde, H. Gardeniers, M. Modestino, D. Fernández Rivas, Influence of bubbles on the energy conversion efficiency of electrochemical reactors, Joule 4 (3) (2020) 555–579, http://dx.doi.org/10.1016/j.joule.2020.01.005.

[9] F. Harnisch, G. Sievers, U. Schröder, Tungsten carbide as electrocatalyst for the hydrogen evolution reaction in pH neutral electrolyte solutions, Appl. Catal. B 89 (3–4) (2009) 455–458, http://dx.doi.org/10.1016/J.APCATB.2009.01.003.

[10] R.C. Sekol, X. Li, P. Cohen, G. Doubek, M. Carmo, A.D. Taylor, Silver palladium core–shell electrocatalyst supported on MWNTs for ORR in alkaline media, Appl. Catal. B 138–139 (2013) 285–293, http://dx.doi.org/10.1016/J.APCATB.2013.02.054.

[11] H. Matsushima, T. Iida, Y. Fukunaka, Gas bubble evolution on transparent electrode during water electrolysis in a magnetic field, Electrochim. Acta 100 (2013) 261–264, http://dx.doi.org/10.1016/j.electacta.2012.05.082.

[12] R.J. Lim, M. Xie, M.A. Sk, J.-M. Lee, A. Fisher, X. Wang, K.H. Lim, A review on the electrochemical reduction of CO_2 in fuel cells, metal electrodes and molecular catalysts, Catalysis Today 233 (2014) 169–180, http://dx.doi.org/10.1016/j.cattod.2013.11.037.

[13] J.E. Funk, J.F. Thorpe, Void fraction and current density distributions in a water electrolysis cell, J. Electrochem. Soc. 116 (1) (1969) 48, http://dx.doi.org/10.1149/1.2411770.

[14] P.J. Sides, Phenomena and effects of electrolytic gas evolution, in: Modern Aspects of Electrochemistry, Springer, 1986, pp. 303–354.

[15] A. Verbruggen, M. Fischedick, W. Moomaw, T. Weir, A. Nadaï, L.J. Nilsson, J. Nyboer, J. Sathaye, Renewable energy costs, potentials, barriers: Conceptual issues, Energy Policy 38 (2) (2010) 850–861, http://dx.doi.org/10.1016/j.enpol.2009.10.036.

[16] X. Zhao, H. Ren, L. Luo, Gas bubbles in electrochemical gas evolution reactions, Langmuir 35 (16) (2019) 5392–5408, http://dx.doi.org/10.1021/acs.langmuir.9b00119.

[17] S. Lubetkin, The motion of electrolytic gas bubbles near electrodes, Electrochim. Acta 48 (4) (2002) 357–375, http://dx.doi.org/10.1016/S0013-4686(02)00682-5.

[18] R. Wedin, L. Davoust, A. Cartellier, P. Byrne, Experiments and modelling on electrochemically generated bubbly flows, Exp. Therm Fluid Sci. 27 (6) (2003) 685–696, http://dx.doi.org/10.1016/S0894-1777(03)00073-6.

[19] R.G. Compton, J.C. Eklund, F. Marken, Sonoelectrochemical processes: A review, Electroanalysis 9 (7) (1997) 509–522, http://dx.doi.org/10.1002/elan.1140090702.

[20] W. Zheng, J.-H. Yong, J.-C. Paul, Simulation of bubbles, Graph. Models 71 (6) (2009) 229–239, http://dx.doi.org/10.1016/j.gmod.2009.08.001.

[21] S.D. Li, C.C. Wang, C.Y. Chen, Water electrolysis in the presence of an ultrasonic field, Electrochim. Acta 54 (15) (2009) 3877–3883, http://dx.doi.org/10.1016/j.electacta.2009.01.087.

[22] A. Zijlstra, D. Fernandez Rivas, H.J. Gardeniers, M. Versluis, D. Lohse, Enhancing acoustic cavitation using artificial crevice bubbles, Ultrasonics 56 (2015) 512–523, http://dx.doi.org/10.1016/j.ultras.2014.10.002.

[23] J.A. da Paz, A. Sales, L.D. da Silva, E.F.M. da Silva, J.A.P. da Costa, M. Navarro, F.D. de Menezes, M. Vilar, Ultrasound-assisted electrocatalytic hydrogenation in water, Appl. Catalysis A: Gen. 550 (2018) 245–255, http://dx.doi.org/10.1016/J.APCATA.2017.11.013.

[24] J. Newman, Scaling with Ohm"s law wired vs. Wireless photoelectrochemical cells, J. Electrochem. Soc. 160 (3) (2013) F309—-F311, http://dx.doi.org/10.1149/2.020304jes.

[25] C. Gabrielli, F. Huet, M. Keddam, A. Macias, A. Sahar, Potential drops due to an attached bubble on a gas-evolving electrode, J. Appl. Electrochem. 19 (1989) 617–629.

[26] H. Vogt, R.J. Balzer, The bubble coverage of gas-evolving electrodes in stagnant electrolytes, Electrochim. Acta 50 (10) (2005) 2073–2079, http://dx.doi.org/10.1016/j.electacta.2004.09.025.

[27] G. Wosiak, M.C. Silva, J. da Silva, E.B. Carneiro-Neto, M.C. Lopes, E. Pereira, Evaluation of interfacial pH change during water splitting at pulsed regime using finite element method, Int. J. Hydrogen Energy 46 (34) (2021) 17644–17652, http://dx.doi.org/10.1016/j.ijhydene.2021.02.195.

[28] P. Van Der Linde, P. Peñas López, A. Moreno Soto, D. Van Der Meer, D. Lohse, H. Gardeniers, D. Fernández Rivas, Gas bubble evolution on microstructured silicon substrates, Energy Environ. Sci. 11 (12) (2018) 3452–3462, http://dx.doi.org/10.1039/c8ee02657b.

[29] S. Jain, L. Qiao, Molecular dynamics simulations of the surface tension of oxygen-supersaturated water, AIP Adv. 7 (4) (2017) http://dx.doi.org/10.1063/1.4979662.

[30] A. Ehrl, G. Bauer, V. Gravemeier, W.A. Wall, A computational approach for the simulation of natural convection in electrochemical cells, J. Comput. Phys. 235 (2013) 764–785, http://dx.doi.org/10.1016/J.JCP.2012.08.043.

[31] J.K. Novev, R.G. Compton, Natural convection effects in electrochemical systems, Curr. Opinion Electrochem. 7 (2018) 118–129, http://dx.doi.org/10.1016/J.COELEC.2017.09.010.

[32] R. Hreiz, L. Abdelouahed, D. Fünfschilling, F. Lapicque, Electrogenerated bubbles induced convection in narrow vertical cells: PIV measurements and Euler-Lagrange CFD simulation, Chem. Eng. Sci. 134 (2015) 138–152, http://dx.doi.org/10.1016/j.ces.2015.04.041.

[33] K.V. Vyakaranam, J.L. Kokini, Prediction of air bubble dispersion in a viscous fluid in a twin-screw continuous mixer using FEM simulations of dispersive mixing, Chem. Eng. Sci. 84 (2012) 303–314, http://dx.doi.org/10.1016/j.ces.2012.07.014.

[34] B. Nearingburg, A.L. Elias, Patterning multilayer microfluidic electrochemical devices by maskless laminar flow lithography, RSC Adv. 4 (57) (2014) 29975, http://dx.doi.org/10.1039/C4RA05106H.

[35] P. Mandin, A.A. Aissa, H. Roustan, J. Hamburger, G. Picard, Two-phase electrolysis process: From the bubble to the electrochemical cell properties, Chem. Eng. Process.: Process Intensif. 47 (11) (2008) 1926–1932, http://dx.doi.org/10.1016/j.cep.2007.10.018.

[36] K. Aldas, N. Pehlivanoglu, M.D. Mat, Numerical and experimental investigation of two-phase flow in an electrochemical cell, Int. J. Hydrogen Energy 33 (14) (2008) 3668–3675, http://dx.doi.org/10.1016/j.ijhydene.2008.04.047.

[37] H. Vogt, O. Aras, R.J. Balzer, The limits of the analogy between boiling and gas evolution at electrodes, Int. J. Heat Mass Transfer 47 (4) (2004) 787–795, http://dx.doi.org/10.1016/j.ijheatmasstransfer.2003.07.023.

[38] A. Alexiadis, M.P. Dudukovic, P. Ramachandran, A. Cornell, On the stability of the flow in multi-channel electrochemical systems, J. Appl. Electrochem. 42 (9) (2012) 679–687, http://dx.doi.org/10.1007/s10800-012-0426-0.

[39] Y. Ding, X. Bi, D. Wilkinson, Numerical investigation of the impact of two-phase flow maldistribution on PEM fuel cell performance, Int. J. Hydrogen Energy 39 (1) (2014) 469–480, http://dx.doi.org/10.1016/j.ijhydene.2013.10.047.

[40] C. Zheng, M. Zhang, S. Qiu, H. Li, T. Wang, H. Wang, Numerical simulation and experimental investigation of gas-liquid two-phase flow in a complex microchannel, Chem. Eng. Sci. 230 (2021) 116198, http://dx.doi.org/10.1016/j.ces.2020.116198.

[41] J.L.C. Santos, V. Geraldes, S. Velizarov, J.G. Crespo, Characterization of fluid dynamics and mass-transfer in an electrochemical oxidation cell by experimental and CFD studies, Chem. Eng. J. 157 (2) (2010) 379–392, http://dx.doi.org/10.1016/j.cej.2009.11.021.

[42] E.J.F. Dickinson, H. Ekström, E. Fontes, COMSOL Multiphysics®: Finite element software for electrochemical analysis. A mini-review, Electrochem. Commun. 40 (2014) 71–74, http://dx.doi.org/10.1016/j.elecom.2013.12.020.

[43] G. Bauer, V. Gravemeier, W. Wall, A 3D finite element approach for the coupled numerical simulation of electrochemical systems and fluid flow, Int. J. Numer. Methods Eng. 86 (2011) 1339–1359, http://dx.doi.org/10.1002/nme.3107.

[44] P.A. Kler, L.D. Dalcin, R.R. Paz, T.E. Tezduyar, SUPG And discontinuity-capturing methods for coupled fluid mechanics and electrochemical transport problems, Comput. Mech. 51 (2) (2013) 171–185, http://dx.doi.org/10.1007/s00466-012-0712-z.

[45] R. Wüthrich, C. Comninellis, H. Bleuler, Bubble evolution on vertical electrodes under extreme current densities, Electrochim. Acta 50 (25-26 SPEC. ISS.) (2005) 5242–5246, http://dx.doi.org/10.1016/j.electacta.2004.12.052.

[46] S.F. Jones, G.M. Evans, K.P. Galvin, Bubble nucleation from gas cavities - A review, Adv. Colloid Interface Sci. 80 (1) (1999) 27–50, http://dx.doi.org/10.1016/S0001-8686(98)00074-8.

[47] J. Hadamard, Mouvement permanent lent d'une sphere liquid et visqueuse dans un liquide visqueux, CR Hebd. Seances Acad. Sci. Paris 152 (1911) 1735–1738.

[48] W. Rybczynski, Uber die fortschreitende Bewegung einer flussigen Kugel in einem zahen Medium, Bull. Acad. Sci. Cracovie A 1 (1911) 40–46.